International Journal of
INTELLIGENT SYSTEMS AND APPLICATIONS IN ENGINEERING
ISSN:2147-6799 www.ijisae.org Original Research Paper

Advancing Alzheimer's Disease Detection: Integrating Machine Learning And Image Analysis For Accurate Diagnosis

[1]Archana Gopinadhan, [2]Dr. Angeline Prasanna G.

Submitted: 03/10/2023 **Revised**: 21/11/2023 **Accepted**: 03/12/2023

Abstract: Alzheimer's disease (AD) has a beneficial global impact on human life despite being a difficult, incurable, and horrible condition. Since it was not preventable by immunization, it was the sixth leading cause of death in the USA. The toughest part of finding new organisms. Understanding the cause of AD and finding ways to prevent or cure it will benefit from the discovery of proteins and genes involved in the illness. They employ practical tools and expertise to investigate the possible interaction between genes/proteins with Alzheimer's. Current information from all known AD proteins/genes was utilized to construct a machine-learning method for protein-connection prediction in Alzheimer's disease. Since MR brain scans are often used for diagnosing Alzheimer's, we suggested the EADD (Enhanced Alzheimer's Disease Detection) method. Multi-layer perceptual (MLP) was used to filter out the background noise in the MRI data set. In this proposed study, we use Histogram equalization to improve images, the Edge-based Robert operator to segment them, CNN with RESNet150 to train them, and the CNN Algorithm to classify them. Based on experimental data, the suggested method in this study has a classification accuracy of up to 98%.

Keywords: *AD, CNN, Classification, EADD, MLP, RESNet150*

1. Introduction

There is a beneficial worldwide effect from Alzheimer's disease (AD), a complex, irreversible, incurable neurological disorder [1]. No vaccines existed against it, making it the sixth leading cause of death in the USA [2]. The biggest challenge in the field of biological research. The identification of proteins and genes relevant to AD will clarify the cause of the illness and lead to the development of vaccines and treatments [3-8]. They use practical tools and knowledge to research Alzheimer's and gene/protein combinations [9]. It is possible to use computational techniques to anticipate the whole set of available genes and proteins linked to AD [10]. Using this data, which includes information on all known AD proteins and genes [11–17], a machine-learning algorithm was developed to provide predictions about which proteins are associated with AD. The precision of the model guarantees the validity of the method. To improve our knowledge of DA and potential vaccinations and therapeutic targets for AD [18-22].

The most prevalent form of dementia, Alzheimer's disease, is characterized by a gradual loss of cognitive abilities and an increase in the difficulty of doing even the most routine of activities. Studies have shown that this deadly illness cannot be treated [23]. By strengthening the patient's quality of life, the disease's course may be slowed, and the patient's cognitive skills may improve [24]. The Enhanced Alzheimer's Disease Detection (EAD) method that has been suggested Alzheimer's disease may often be diagnosed using magnetic resonance imaging of the brain. The suggested system employs a multi-layer perceptron (MLP) with histogram equalization for noise reduction, an edge-based Robert operator for segmentation, a CNN ResNet 150 network for training, and a CNN Algorithm for classification. This opens up several avenues for advancing and bettering diagnostics via the use of image recognition methods. Medical professionals may save time and effort with automatic identification of any disease sample. The noises emitted during operation complicate the development of an automated system for disease diagnosis based on photographs of human anatomy [25]. The current state of segmentation algorithms makes it challenging to automatically diagnose Alzheimer's disease [26].

Therefore, it is vital to develop automated Alzheimer's diagnosis technology that is both accurate and rapid [27-31]. The diagnosis of Alzheimer's disease often involves the use of brain volume calculations based on anatomical imaging. The goal of this research is to develop an automated system for identifying Alzheimer's disease based on texture changes in the hippocampus using MRI. CT scans reveal shrinkage of the cortex in Alzheimer's disease patients [32]. Accurate interpretation of CT scan pictures is also crucial for the early identification of

[1]*Research Scholar, Department of Computer Science, AJK College of Arts and Science, Coimbatore- 641 105.Email: archanagopinadhan@gmail.com*
[2]*Former Associate Professor and Head, Department of Computer Science, AJK College of Arts and Science Coimbatore- 641 105. Email: angelineprasanna.g@drngpasc.ac.in*

Alzheimer's disease. Edge detection is used to find CT image artifacts. In order to assess breaks in grayscale pictures, edge detection is a crucial initial step in image processing. Structural MRIs with small samples and few scan layers are often used in clinical practice. However, relevant data is necessary for in-depth study. Using a weighted mixture of positive and negative samples and an approach for learning a limited number of pieces, the authors of this work propose an enhanced data set system relevant to the functional criteria for the clinical diagnosis of Alzheimer's disease [33]. The model's ability to generalize is improved, and the finer points of the image are enhanced as a consequence.

The main Contributions of this paper are as follows

- MRI image Noise removal has been done with MLP
- Image enhancement using CLAHE with histogram equalization
- Image segmentation has done with Robert Operator
- Image data trained CNN with RESNet150
- AD Multiclass classification using CNN algorithm.

In the next sections of the study, we will examine the current methodologies for identifying AD. In Section 3, we see the EADD model in action. The findings and discussion of the EADD model are summed up in Section 4. The conclusion and recommendations for further research are presented in Section 5.

2. Background Study

Akhila D B et al. [1] It was suggested that Elman backpropagation be used to categorize the various forms of AD diagnostic criteria. By using an affine transform, PET and MRI were able to merge two distinct methods of categorization. After obtaining features using GLCM, classifying them with an Elman BP network, and evaluating their efficacy. Our suggested technique has shown superior performance, making it ideal for real-world applications and providing precise diagnosis of AD.

A, S., Bhattacharjee, et al. [3] We researched and evaluated MR brain pictures to categorize neurodegenerative disorders. This research focuses mostly on classifying Alzheimer's disease using photographs of healthy controls. We studied brain MR images available from the OASIS database, which is open to the public. The input image is subdivided at each decomposition level into many mother wavelets (Haar, Symlet, and db2), and fractal features are recovered at each level. Many classifiers use these traits to identify Alzheimer's from healthy controls. Experiments demonstrate that the SVM classifier with the symlet wavelet feature yields greater performance. Rank effectiveness and minimum processing times, Blanchette et al. [7] These formulas allow us to identify at-risk individuals for AD based on their performance in driving simulators. These findings highlight the value of driving as a proxy for cognitive health and suggest further research into the potential of VR driving as a diagnostic tool for AD. Machine learning may be an essential tool when planning future studies to identify signs of cognitive decline.

Fedorov et al. [11] A prediction study for the development of Alzheimer's disease yields results that are on par with those produced using supervised techniques. We want to expand our study population and investigate more diseases in the near future. The potential for our model's prediction power to be improved by future research into the multimodal integration of brain imaging data is intriguing.

Gunawardena et al. [13] Can early Alzheimer's disease signs be detected using Neuroimaging data using deep learning techniques like CNNs? The first experiment shows that the SVM method previously used to identify people with moderate to severe AD symptoms is inadequate. AD, MCI, and NL may all be detected early with the use of image categorization. Despite this, SVM is terrible at categorizing certain types of data.

Kaur, H., and Rani, J. [17] provide a quick and effective method for fine-tuning the brightness of a picture. Brightening an image using LRE, ARE, or CLARE is also helpful. Since CLARE doesn't need as much time investment, it is preferable than LRE. CLARE is used to improve contrast and remove noise from a picture, although it may also generate new noise artifacts.

Li, C., Fang, et al. [18] To find Alzheimer's disease-related genetic variants, we developed and validated an image feature extraction strategy. Using a support vector machine (SVM) based learner, the associations between imaging and AD in each brain area were recorded. The splits regression model was then used to select the genetic variants related with AD. The proposed model may be used to understand a wide range of neurological conditions.

Sathish Kumar, L. et al. [23] A unique approach was developed to detect AD even in the MCI phase. The proposed method automatically extracts the most common MRIs by using a well-designed classification architecture and a pre-trained AlexNet network. This technique has the potential to identify some chronic disorders, such as Parkinson's. When Alzheimer's disease is detected early, therapy may start before significant brain volume is lost. Researchers are working to create new models of beta-amyloid protein aggregation and tau, a known predictor of Alzheimer's disease, in an effort to

better understand the illness and its causes. Also, we'll be done with this soon.

Wang S. et al. [31] To examine MR brain scans for indicators of Alzheimer's disease and mild cognitive impairment, our team developed a collection of highly linked 3D convolutional networks. Alzheimer's disease (AD) and moderate cognitive impairment (MCI) may be treated in different ways because of their distinguishable diagnostic features. We address the issue of insufficient training data by using dense connections in 3D-CNN. It is easier to train with fewer parameters on a densely linked network because to the increased efficiency with which information and gradients are sent. Different 3D settings were tested extensively to see how they impacted DenseNet's performance.

a) Problem Formation

Opportunities in medical imaging science have expanded thanks to recent technological and imaging developments. As part of the evaluation, photographs were taken, including some that were taken unattended after a preliminary diagnosis had been made. The likelihood of an image-driven healthcare data mining study is increased by the wide variety of digital image resources available. Medical image data encoding, retrieval, alteration, and display are all open to investigation. JPEG files of brain MRI scans provide private information about patients and their tumors. Rapid and efficient collection of medical imaging data is essential. A skilled image processor will study, interpret, collect, and analyze significant visual information. Each patient had many pictures taken of them throughout the exam, and those pictures were used to make a diagnosis. Manually extracting critical information from several medical images requires substantial work from medical professionals. It's a huge roadblock.

The second problem with manual segmentation is that it relies on the expertise of a single individual to determine where features begin and end. Even the same doctor may have various conclusions about the same imaging in different settings. Leaving out any pixels related to tumors might be detrimental to a patient's health. Another issue is that there is no access to a specialist physician. Specialists are in short supply in some underserved areas and small towns. Imagine a situation in which a person diagnoses and treats a sickness early with the help of a remote physician and a digital picture transmission. In any case, it will improve the lives of those who live in rural areas.

After recognizing the shortcomings of current segmentation and classification approaches for brain tumor MRI images, this investigation indicated the need for an effective storage optimization model for classification storage and segmentation. This study offers a new imaging paradigm that may significantly enhance brain MRI picture preservation. The model is able to analyze, store, and classify MRI images of benign and malignant brain tumors.

3. Material And Methods

The EADD model is a suggested tool for making early diagnoses of AD. We use an MLP to filter out background noise, a hybrid deep learning technique to train our models, and a convolutional neural network to classify them.

3.1: Dataset description:

The MR imageon this page may be used to build a diagram of the brain's architecture, including the medulla oblongata, emphasizinginput structure. Many parts of a picture may be identified individually. The proposed work is executed on AD-related datasets obtained from the https://www.kaggle.com/datasets/tourist55/alzheimers-dataset-4-class-of-images website link.

Fig 1: input image

Figure 1 illustrates the RAW Input image used directly with preprocessing procedures and data sharpening.)

3.2NOISE REMOVINGUSING MLP

Preliminary picture processing of many kinds is required. Clarifies photos by removing background noise. The brain is more sensitive than other organs, thus imaging of it should be as clear and as free of noise as possible. In

this case, the MLP technique was used to do picture denoising.

3.2.1 Multilayer Perceptron(MLP).

One kind of supervised classifier is the multilayer perceptron. These neural networks are feed forward and are trained using a back propagation technique. Common parts include an input layer, an output layer, and a layer or levels that are hidden from view. In cases when an algorithmic answer is unavailable or cannot be precisely specified, MLP is used. It is via training that an MLP learns to transform input data into the desired output. Pattern recognition and interpolation are two common applications of MLP. MRI and other imaging modalities are utilized for MLP diagnosis of AD. Three hidden layers and three neurons per layer are discovered to be the ideal values when the network is built using a variety of settings for these parameters. The network has been trained at a rate of 0.3 learning.

$NR = MRI(3.hd + 3n)$ ---------- (1)

Eq (1) denotes the noise removal process has done with MRI and 3 hidden layer and 3 neuron with each layer.

3.3HISTOGRAM EQUALIZATION

By lowering the slope of the contrast transformation function by merely restricting the histogram amplitude at particular grey levels, we may reduce contrast overshoot at grey levels that occur often. To restrict the amplitude of the histogram at grey levels with a high frequency of recurrence, the histogram is clipped at a threshold 'T' where,

$T=\left[\frac{1}{L}\sum_{K=0}^{L-1} P_K\right]+\left[P_{max} - \frac{1}{L}\sum_{K=0}^{L-1} P_K\right]\alpha \quad 0\leq\alpha\leq1$ ---------- (2)

Where $'P_k'$ is the discrete probability density of the K^{th}grey level in the image 'X 'histogram bin, and a 'is the clip limit. Threshold the 'T 'is determined directly from the value of the clip-limit .' a 'as evident in equation (2) possible range of the threshold is between the mean height of the histogram and maximum height,' P_{max} 'of the histogram such that,

$\lim_{\alpha\to0} T=\frac{1}{L}\sum_{K=0}^{L-1} p_k$ and $\lim_{\alpha\to1} T=P_{max}$---------- (3)

Clipping the original histogram 'P' at the threshold, 'T' yields

The area under the curve is normalized by reassigning the clipped pixels to the bins of the clipped histogram 't '. Both the total number of clipped pixels and the percentage of empty space in the bin are needed to get an accurate estimate of the number of pixels removed from the histogram. During clipping, the complete number of pixels was deleted from the histogram,

$n_c=\sum_{K=0}^{L-1}(p_{k-}t_k)$=MN-$\sum_{K-0}^{L-1} t_k$----------(4)

Vacancy 'Vk,' in the K^{th} the bin of the histogram obtained after the clipping process 't' is,

V_k=1– $(\frac{t_k}{T})$ ----------(5)

The number of pixels refilled in or allotted back to each bin of the clipped histogram depends on the 'relative vacancy' in it. relative vacancy 'f_k', in the K^{th} process, 't' is a fraction of vacancy 'vk' in it and total vacancy available in different bins of the clipped histogram as,

$f_k=\frac{v_k}{\sum_{K=0}^{L-1} v_k}$---------- (6)

Number of pixels 'd_K', put back to the $K^{th}the$ bin of the histogram after clipping is a fraction $'f_k'$ of the total quantity of the clipped pixels, $'n_c'$,

$d_K=n_c f_k$---------- (7)

As the residue pixels received as a result of the clipping process are refilled completely into the bins of the clipped histogram, the area under the curve of the new histogram, 'h' grow back to that of the original histogram 'P,' satisfying the constrain,

$\sum_{K=0}^{L-1} h_k = \sum_{K=0}^{L-1} k\, P_K$ ---------- (8)

In MR images, it is not uncommon to see large background patches. Due to the presence of the black background region, the amplitude of the new histogram in Equation (8) at zero grey level, h (k)at k=0, 'h 0', will be quite large, either ho=T or ho>>0.

3.3.1 Convolutional shape local binary texture:

A high-contrast, grayscale image is first determined, and then the image is re-formatted such that each pixel displays the correct information at the correct moment. The same highlighted data view will show an image where preprocessed image data has been prepared for a clustered area. The presence of a local and global cluster head for all data in the matrix structure is indicative of its calculation as an array. The method starts off with a classification of local binary bit patterns and textures. New clusters and heads often appear in the vicinity of the dispersed population. We focus on the significance of the central strength region that is independent of the matrix in this work. Based on the optimal results, each typical regional head is evaluated and highlighted in a single array. The necessary matrix strength core data must be obtained autonomously in order to identify afflicted areas from unaffected ones.

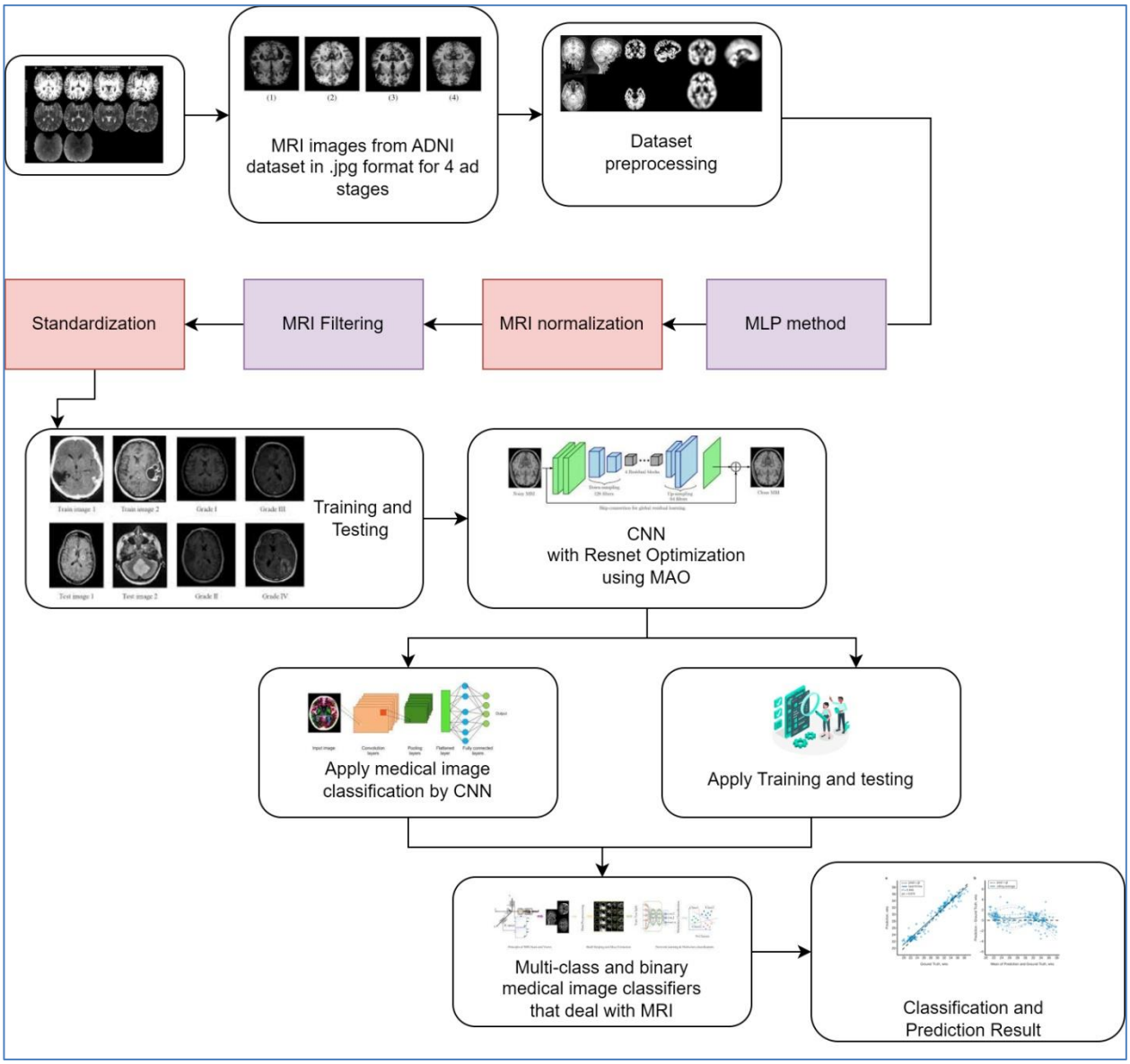

Fig 2: EADD Architecture for Early AD Preditcion

The suggested workflow is shown in Figure 2, and the data for the classification function is created and displayed as a binary texture pattern. When the numbers from each group are added together, it yields a number that serves as an average for this area. Based on the input function, the highlighted area ought to be more expansive and brighter.

3.4 Edge-based Image Segmentation

Once its epicenter has been located, the region of interest may be marked and studied in further detail. Each pixel's brightness is controlled by this picture. Cropping an image results in the assignment of a white or black value to each pixel in the picture. The images depict both healthy white tissue and dark, rotting tissue. A healthy patient should have a negligible amount of dark pixels. The amount of white and black pixels in a brain scan is used to diagnose the patient with moderate cognitive impairment, Alzheimer's disease, or a stable mental state.

3.4.1 Clustering Methods:Clustering techniques may separate an image into groups of equally bright pixels or voxels without the need of training pictures. Clustering methods are trained using publicly accessible picture data. Segmentation and preprocessing occurred in two steps at the same time: Cluster analysis and tissue type estimate prediction.

$$j_m = \sum_{i=1}^{c} \sum_{j=1}^{N} u_{ijD_{ij}}^{m} \text{---------- (9)}$$

The degree of uncertainty in the final split is controlled by the weighting exponent M (often set to m = 2; k-means clustering is used if m = 1). When comparing cluster centers vi and xj, the similarity measure is denoted by dij.

Each cluster is illuminated independently, depending on its location. The morphological picture shown in Figure 8 has a moderate filter rate, poor homogeneity data, and a high noise cancellation rate.

Thresholding

Thresholding is often used to divide up images. Segmentation in this case is done using grayscale or pixel density. It's a cutoff for sorting pixels in a picture by color and luminance, respectively.

Roberts Cross Operator

The 2-D spatial gradient of an MRI picture may be quickly and easily measured using the Roberts Cross operator. Due to its inability to identify edges with angles that are multiples of 45 degrees and its inconsistent behavior on both sides, this detector is seldom used. The identical operator is used as the input to this function.

Its gradient magnitude is given by:

$$\nabla f = mag(\Delta F) = [GX^2 + GY^2]^{1/2} \quad \text{----------} \quad (10)$$

When a spatial gradient is produced, its onset angle is determined by:

$$\theta = \arctan\left(\frac{Gy}{Gx}\right) - 3\pi/4 \quad \text{----------} \quad (11)$$

The operation or condition of components is a function of this net input.

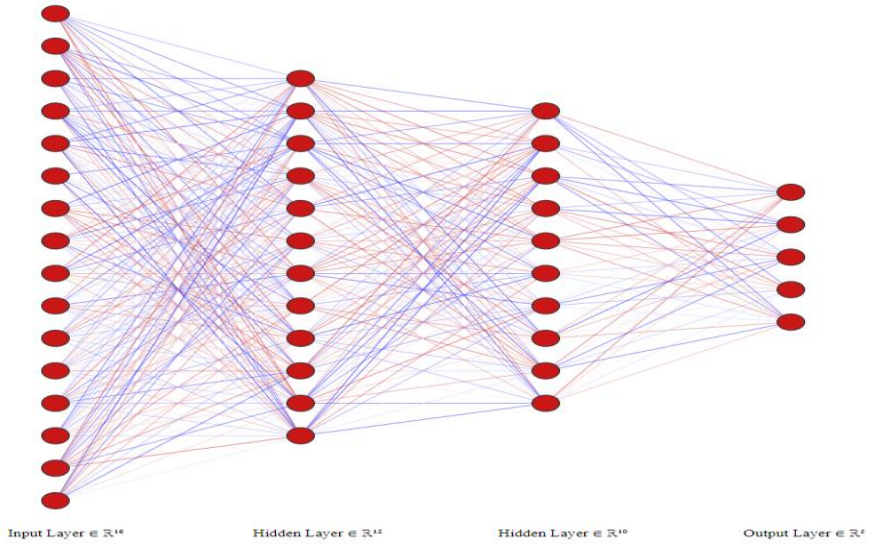

Fig 3: CNN Layers with the Input layer, hidden layer, and output layer

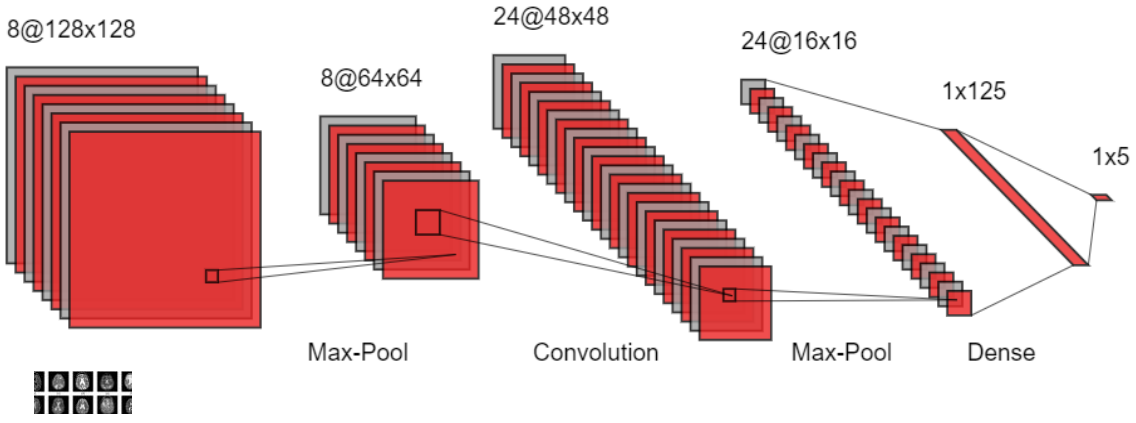

Fig 4: Convolutional Neural network with Densenet architecture

3.5 Training and Testing

Convolutional Neural Networks (CNNs) have recently surpassed Deep Neural Networks (DNNs) as the preferred approach for image recognition and other computer vision applications. Figures 3 and 4 show the basic structure of a typical convolutional network. The hidden activation hi at a given layer in a fully connected network is calculated by multiplying the complete input

X by the layer's weights W. In contrast, a convolutional neural network (CNN) calculates its hidden activation by multiplying a portion of the input (e.g. [x1, x2, x3]) by the weights W assigned to the layer in question. Since activations for the convolutional layer bands have already been calculated by the hidden unit, the activations delivered to the Max-pooling unit originate from the convolutional layers. The hidden units' activations are averaged out and the maximum is returned by the max-pooling layer. We implemented our solution using RESNet150's convolutional and fully linked network layers. Convolutional layers in the aforementioned network will help reduce spectral spread. CNN with RESNet150 has "local and global pooling" layers that provide some translation invariance.

$h^{(s)} = f_h\left(A_{hh}h^{(s-1)} + A_{ih}x^{(s)}Wish(s) + b_h\right)$ ---------- (12)

$y^{(s)} = f_0\left(A_{ho}h^{(s)} + bo\right)$ ---------- (13)

Where

X^s - the input data

h^s - the hidden layer units

y^s - the output

$A_{ih'}, A_{hh} and A_{ho}$ - the transformation matrices between $X^{(s)}\&h^{(s)}, h^{(s-1)}\&h^s and h^{(s)}\&y^s$

$b_h and b_o$ - the constant bias terms

$f_h and f_o$ - the no-linear activation function

By updating Aih, Ahh, and Aho, RESNet are able to remember all the previous data and utilize it to understand the relationships between image regions at different spatial locations, also known as spatial dependences. In order to maximize the DNN's performance, the image from the CNN layer is converted into a four-dimensional spatial sequence to absorb the context in all sections of the image.

Referring to Equation (13), the quad-directional DNN is defined as

$h_{\rightarrow}^{(s)} = f_h\left(A_{hh\rightarrow}h_{\rightarrow}^{(s-1)} + A_{ih\rightarrow}x^{(s)} + b_{h\rightarrow}\right)$ ---------- (14)

$h_{\uparrow}^{(s)} = f_h\left(A_{hh\uparrow}h_{\uparrow}^{(s-1)} + A_{ih\uparrow}x^{(s)} + b_{h\uparrow}\right)$ ---------- (15)

$h^{(s)} = h_{\rightarrow}^{(s)} + h_{\leftarrow}^{(s)} + h_{\downarrow}^{(s)} + h_{\uparrow}^{(s)}$---------- (16)

Where

$h_{\rightarrow}^{(s)}$ -the left-to-right hidden layer units

$h_{\leftarrow}^{(s)}$ -the right-to-left hidden layer units

$h_{\downarrow}^{(s)}$ - the top-to-bottom hidden layer units

$h_{\uparrow}^{(s)}$ - the bottom-to-top hidden layer units

The summation of these four is $h^{(s)}$.

Multi-directional DNN sequences' forward and reverse unfolding processes have their weights modified.

Two completely linked layers are defined as follows to gather all the hidden units in the DNN layers:

g = $f_g\left(A_{hg}H + b_g\right)$ ---------- (17)

y = $f_y\left(A_{gy}g + b_y\right)$ ---------- (18)

Where

A_{hg} - transfer matrix for the concatenated DNN outputs H to the global hidden layer g.

A_{av} _ transfer matrix for g to the predicted class lable y

$b_g\&b_y$ - the bias value

$f_g\&f_y$ - non-linear activation function and softmax

The recurrent convolutional layer (RCL) is the key part of RCNN. The net input x_{ijk} (t) at discrete time step t of RCL at (I,j) on the k^{th} feature map is given by

$X_{ijk}(t) = (A_k^f)^T u^{(i,j)}(t) + (A_k^r)^T v^{(i,j)}(t-1) + b_k$ ---------- (19)

Where

$u^{(i,j)}(t))$ - the feed-forward input

$v^{(i,j)}(t-1)$ - the recurrent input

A_k^f - feed-forward weights

A_k^r - recurrent weights

b_k - bias

In the above Equation, the first part is the same as in CNN, and the second is from the recurrent connection. Both parts of the Equation are centered at (I,j)

Some function of this net input is the activity or state of RCL, which is given by

$z_{ijk}(t) = f(g(X_{ijk}))$ ---------- (20)

$$f\left(g\left(x_{ijk}\right)\right) = \frac{g(x_{ijk}(t))}{\left(1+\frac{a}{n}\sum_{k'=\max\left(0,k-\frac{n}{2}\right)}^{k'=\min\left(K,k+\frac{n}{2}\right)}(g(x_{ijk'}(t)))^2\right)\beta}$$ ---------- (21)

The number of feature mappings in the current layer is denoted by k, and the normalization constants and are given.

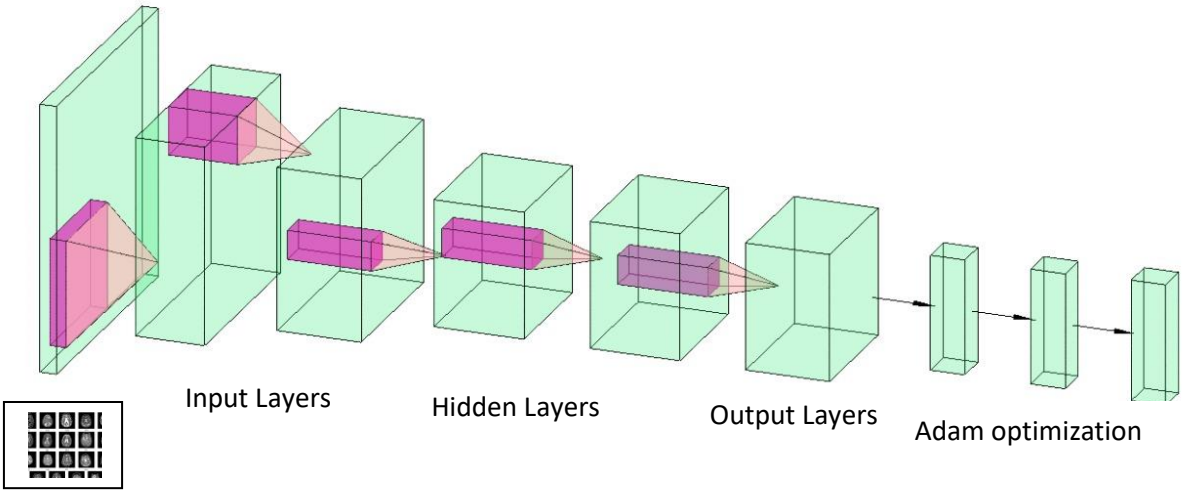

Fig 5: Proposed Hybrid neural network architecture with optimization and multi-class classification

3.6 EARLY ALZEIMERS DISEASE PREDICTION USING CNN

Step1: acquire the image's dimensions from the source and reformat it into a more conventional form.

Step2: Choose the Multi-Layer Perceptron (MLP) filter to locate the image's window region (rectangular window), then reposition the window to eliminate noise from images of varying sizes and shapes.

Step 3: The picture with disc form (5, 2) is enlarged and corroded before being applied to a binary image.

Step 4: I :d area (0,1), a low-intensity portion of the pi ıced (256,256)

Step 5: Images are divided into fragments of various dimensions (3,3) and arranged in a single-dimensional array.

Step 6: Get the midpoint of the 1d array (to have a highly attractive region)

In Step 7, LBP is calculated using the maximum of the average means as a reference (avg mean)

In the eighth step, high-energy data is employed as a standard against which generalized features of AD images are calculated for all possible values of w (window size).

Step 9: The image index is reset to 1 based on the window size data (new index x = 1 as a reference is taken to persist in the picture).

Input to the image is complete at step 10 with the sum of features (f).

Convolutional neural networks are the next step.Input layers → size of image structure is given as one of the input

A. A. The images in each group are classified according to their dimensions, which range from zero to one.
B. B. The convolution, pooling, dense, and output layers are each trained independently in their respective domains.
C. Every layer of information feature with array matrix
D. Each array matrix has neurons and connected layers and has an equality label
E. The knowledge base and knowledge graph of the structure are defined, then the collective field as (s) is noted
F. Feature data s = i+o layer,

Step 12: multi-class classification with early prediction of AD

Step 13: End of the process

3.6.1 MODIFIED ADAM OPTIMIZATION

1. First, Adam mode alignment data are unavailable.
2. Iterating the data is essential for both monitoring and forecasting data.
3. Third, the model does not choose an iteration based on this input (dataset)
4. Finding the model's fitness function
5. 5. The model iteration will start, and the goal function of the model will be selected.
6. Test rats will be exposed to both higher and lower levels of energy.
7. Seven. We investigate data and random numbers to determine whether they fall within this range.

8. 8 If the global fitness data search bit matches, the model's energy calculation will be updated by randomly hopping from one model to the next.
9. Keys for the energy data required to validate the model require a complicated computation of high and hard data (grouped to produce numerous data).
10. The emergence of an optimized layer allowing for the recovery of important data has allowed for the calculation of comprehensive data, including high energy mode vector data, in a very efficient manner.
11. Eleven The data's tolerance is determined, and the maturity of identifying the segmented component, just as in the result.

Synapses link the brain's estimated 100 billion nerve cells together. As people become older, their brains develop plaques and tangles. They start in the brain's memory hub, the hippocampus, then expand outward. Damage to nerve cell function is caused by the cessation or disruption of communication between neurons as a result of the accumulation of plaques and tangles. Alzheimer's disease is characterized by a deterioration in cognitive abilities, aberrant behaviors, and an inability to carry out routine activities because nerve cells have been damaged or died.

4. Experimental Results And Discussion

Python programming, specifically version 3.8, was used to realize the suggested paradigm. This chapter presents the findings from the experiments. Training and testing have made use of CNN-ResNet deep neural networks. Table 1 displays the outcomes of model training and testing.

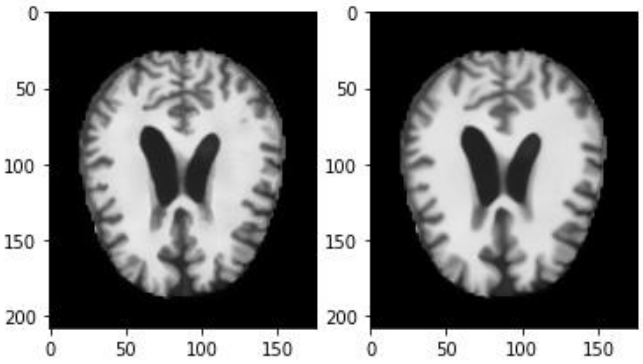

Fig 6: Image Noise Removal using MLP

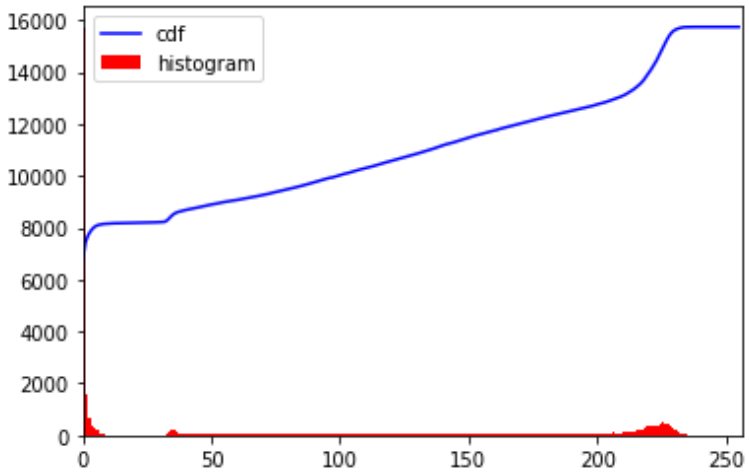

Fig 7: Histogram equalization using CDF function

The MLP Algorithm is used to reduce noise from MRI images, and the results are shown in Figure 6. Figure 7 shows the work that histogram equalization applied on the Cumulative Density Function (CDF).

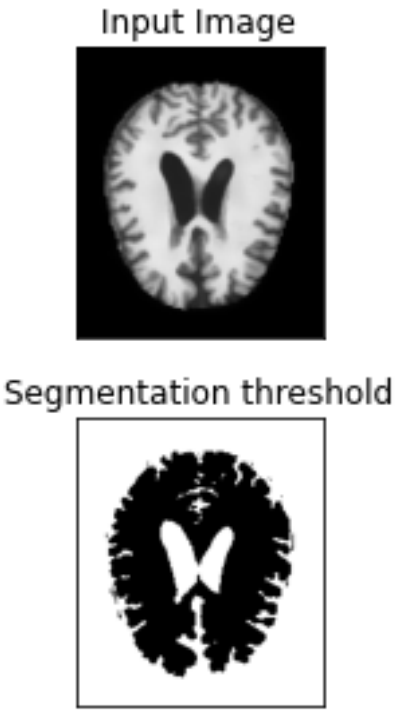

Fig 8: Image Segmentation

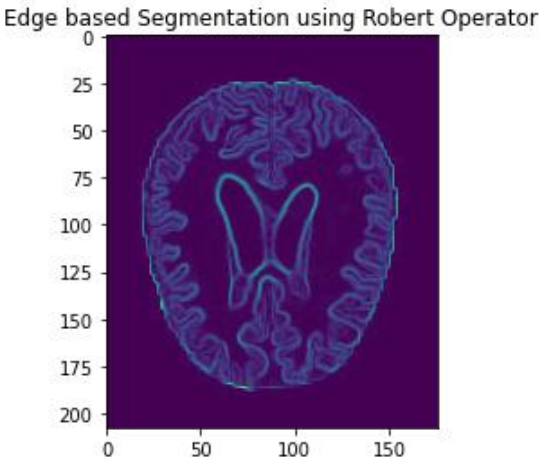

Fig 9: Edge based Segmentation using Robert operator after segmentation

The input MRI image and the segmentation threshold has shown in figure 8. And the proposed Robert operator with edgebased segmentation results has shown in figure 9.

Table 1: Training and testing values with the 10 Epoch

Epoch	Training Loss	Validation Loss	Training Accuracy	Testing Accuracy
1	00.3756	00.2131	00.8971	00.94
2	00.1800	00.1533	00.9490	00.96
3	00.1377	00.1300	00.9613	00.96
4	00.1054	00.1106	00.9689	00.97
5	00.0871	00.1014	00.9751	00.97
6	00.0733	00.0954	00.9785	00.97
7	00.0627	00.0936	00.9815	00.97

8	00.0541	00.0849	00.9843	00.97
9	00.0469	00.0850	00.9869	00.97
10	00.0405	00.0823	00.9883	00.98

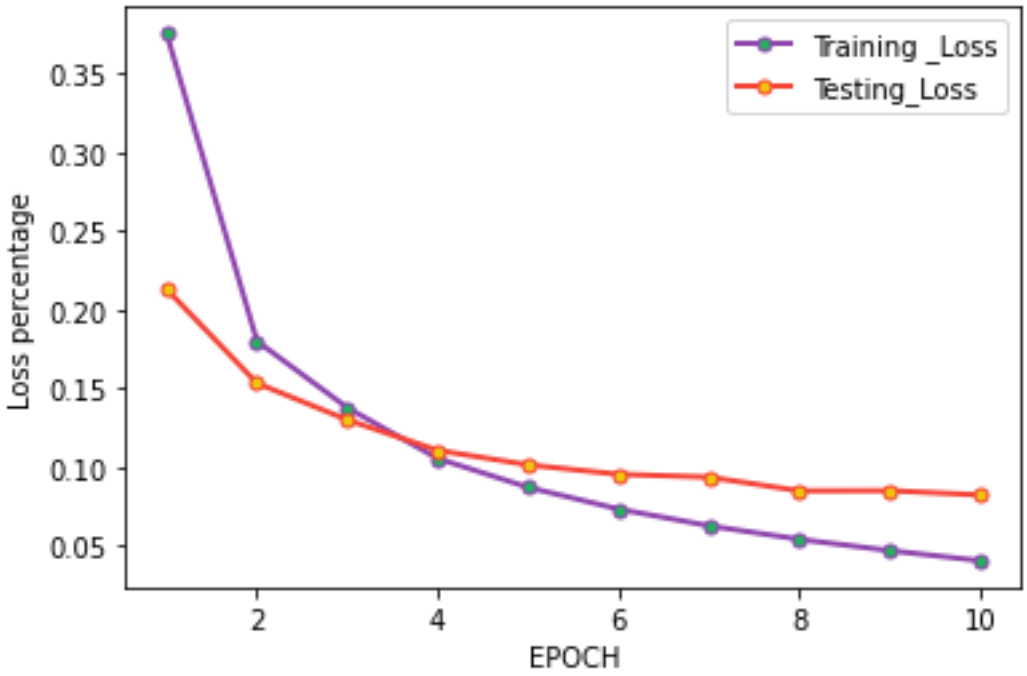

Fig 10: Training and testing loss

The loss values in Figure 10 illustrate the proposed model's training progress across numerous epochs. The X-axis depicts the epoch number, which signifies how many times the model has traversed the complete training dataset. The Y-axis indicates the loss value, which quantifies the difference between the model's expected and actual output.

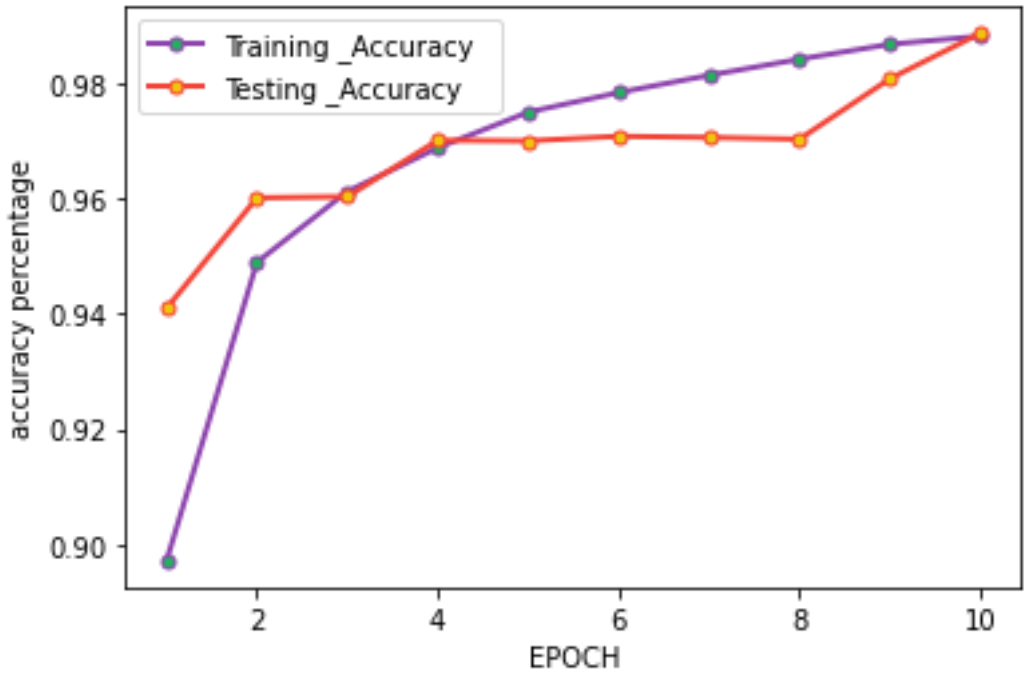

Fig 11: Training and testing Accuracy.

Figure 7 depicts the performance of the trained CNN-ResNet model on a different testing dataset after each epoch throughout the training procedure. The X-axis displays the epoch number, which indicates how many times the model has traversed the whole training dataset and changed its parameters. The accuracy, shown by the Y-axis, is a measure of how effectively the model predicts the proper labels for the testing data.

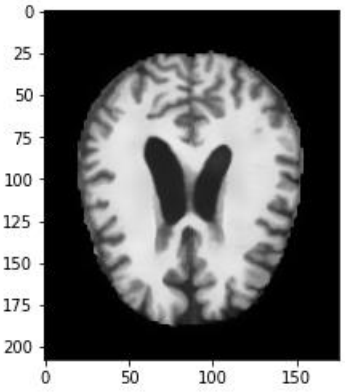

Fig 12: Input MRI Image it will predicted by Moderate Demented

The input MRI image has predicted by using proposed model with Moderate Demented output is shown in figure 12.

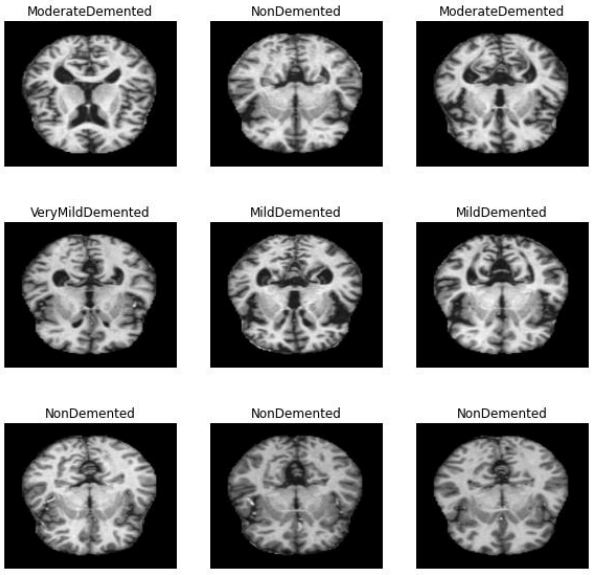

Fig 13: CNN Image Classification

The proposed model schives 98% accuracy. And the CNN has classified the MRI image as multi-class classification is shown in figure 13.

5. Conclusions and Future Work

To better anticipate the onset of AD, we put forward the EADD architecture. Brain shrinkage and enlarged blood vessels. Vascular/tumor sizes may be determined with the use of image segmentation. The degree of enlargement may indicate the existence of mild cognitive impairment, early Alzheimer's disease, moderate Alzheimer's disease, or advanced Alzheimer's disease. Alzheimer's disease may also be detected in part by assessing how much brain shrinkage has occurred. In this research, a system for spotting signs of AD at an early stage was presented. MLP is used to filter out unwanted sounds in MRI scans, and an Edge-based Robert operator was used to divide the images into distinct regions. Resnet150 was used for the training process. In this categorization, CNN was used. According to the findings, using boosts classification precision. The proposed method reaches 98% accuracy, allowing it to overcome the problem of early diagnosis without resulting in brain damage. Medical imaging research will be aided by this. The long-term goal of this research is to create a paradigm shift in telemedicine by automating the model and putting it into practice in a distant setting.

Reference

[1] Akhila D B, Shobhana S, Fred, A. L., & Kumar, S. . (2016). Robust Alzheimer's disease classification based on multimodal neuroimaging. 2016 IEEE International Conference on Engineering and

Technology
(ICETECH). doi:10.1109/icetech.2016.7569348

[2] Burgmans, S., van de Haar, H., van Osch, M., Jansen, J., van Buchem, M., Hofman, P., … Backes, W. (2014). Blood-Brain Barrier Leakage In Alzheimer's Disease: A Dynamic Contrast-Enhanced MRI Study. Alzheimer's & Dementia, 10(4), P101. doi:10.1016/j.jalz.2014.05.188

[3] A, S., Battacharjee, P., Prasad I, A., & Sanyal, G. (2018). Brain MR Image Analysis using Discrete wavelet Transform with Fractal Feature Analysis. 2018 Second International Conference on Electronics, Communication and Aerospace Technology
(ICECA). doi:10.1109/iceca.2018.8474806

[4] Beagum, S. S., Almas, A. A., & Sheeja, S. (2016). Alzheimer's disease, bio-markers, and the role of classification techniques in early diagnosis from neuro-images — An analysis. 2016 IEEE International Conference on Computational Intelligence and Computing Research (ICCIC). doi:10.1109/iccic.2016.7919701

[5] Bakkouri, I., Afdel, K., Benois-Pineau, J., & Catheline, G. (2019). Recognition of Alzheimer's Disease on sMRI based on 3D Multi-Scale CNN Features and a Gated Recurrent Fusion Unit. 2019 International Conference on Content-Based Multimedia Indexing (CBMI). doi:10.1109/cbmi.2019.8877477

[6] Burgmans, S., van de Haar, H., van Osch, M., Jansen, J., van Buchem, M., Hofman, P., … Backes, W. (2014). Blood-Brain-Barrier Leakage In Alzheimer's Disease: A Dynamic Contrast-Enhanced MRI Study. Alzheimer's & Dementia, 10(4), P557. doi:10.1016/j.jalz.2014.05.903

[7] Blanchette, R., Khojandi, A., Cox, D., Oliver, M., & Fernandez, R. (2020). Predicting Alzheimer's Disease Using Driving Simulator Data. 2020 42nd Annual International Conference of the IEEE Engineering in Medicine & Biology Society (EMBC). doi:10.1109/embc44109.2020.9176118

[8] Chelsy Sapna Josephus, & Remya, S. (2011). Multilayered Contrast Limited Adaptive Histogram Equalization Using Frost Filter. 2011 IEEE Recent Advances in Intelligent Computational
Systems. doi:10.1109/raics.2011.6069388

[9] Chauhan, G., Adams, H. H. H., Bis, J., Weinstein, G., Yu, L., Smith, A., … Debette, S. (2014). Association Of Alzheimer Disease Gwas Loci With MRI-Markers Of Brain Aging. Alzheimer's & Dementia, 10(4), P258. doi:10.1016/j.jalz.2014.04.406

[10] Matthews, D. C., Andrews, R. D., Lukic, A. S., Mishra, V. R., Banks, S. J., Cummings, J. L., & Bernick, C. (2018). *MRI* Classifiers Characterize Mild Traumatic Brain Injury In Symptomatic And Presymptomatic Stages And Differentiate From Alzheimer's Disease–Related Impairment. *Alzheimer's & Dementia, 14(7), P443–P445*. doi:10.1016/j.jalz.2018.06.388

[11] Fedorov, A., Hjelm, R. D., Abrol, A., Fu, Z., Du, Y., Plis, S., & Calhoun, V. D. (2019). Prediction of Progression to Alzheimer's disease with Deep InfoMax. 2019 IEEE EMBS International Conference on Biomedical & Health Informatics (BHI). doi:10.1109/bhi.2019.8834630

[12] Falangola, M. F., Jensen, J. H., Tabesh, A., Hu, C., Deardorff, R. L., Babb, J. S., … Helpern, J. A. (2013). Non-Gaussian diffusion MRI assessment of brain microstructure in mild cognitive impairment and Alzheimer's disease. Magnetic Resonance Imaging, 31(6), 840–846. doi:10.1016/j.mri.2013.02.008

[13] Gunawardena, K. A. N. N. P., Rajapakse, R. N., & Kodikara, N. D. (2017). Applying convolutional neural networks for pre-detection of alzheimer's disease from structural MRI data. 2017 24th International Conference on Mechatronics and Machine Vision in Practice (M2VIP). doi:10.1109/m2vip.2017.8211486

[14] Herrera, L. J., Rojas, I., Pomares, H., Guillen, A., Valenzuela, O., & Banos, O. (2013). Classification of MRI Images for Alzheimer's Disease Detection. 2013 International Conference on Social Computing. doi:10.1109/socialcom.2013.127

[15] Jang, J.-W., Park, S. Y., Park, Y. H., Baek, M. J., Lim, J.-S., Youn, Y. C., & Kim, S. (2014). A Comprehensive Visual Rating Scale On Brain MRI: Application To Alzheimer's Disease, Mild Cognitive Impairment, And Subjective Memory Impairment. Alzheimer's & Dementia, 10(4), P714. doi:10.1016/j.jalz.2014.05.1319

[16] Josephs, K. A., Dickson, D. W., Murray, M. E., Senjem, M. L., Parisi, J. E., Petersen, R. C., … Whitwell, J. L. (2013). Quantitative neurofibrillary tangle density and brain volumetric MRI analyses in Alzheimer's disease presenting as logopenic progressive aphasia. Brain and Language, 127(2), 127–134. doi:10.1016/j.bandl.2013.02.003

[17] Kaur, H., & Rani, J. (2016). MRI brain image enhancement using Histogram Equalization techniques. 2016 International Conference on Wireless Communications, Signal Processing and Networking
(WiSPNET). doi:10.1109/wispnet.2016.7566237

[18] Li, C., Fang, C., Adjouadi, M., Cabrerizo, M., Barreto, A., Andrian, J., … Loewenstein, D. (2017). A Neuroimaging Feature Extraction Model for Imaging Genetics with Application to Alzheimer's Disease. 2017 IEEE 17th International Conference on Bioinformatics and Bioengineering (BIBE). doi:10.1109/bibe.2017.00-85

[19] Matthews, D. C., Andrews, R. D., Lukic, A. S., Mishra, V. R., Banks, S. J., Cummings, J. L., & Bernick, C. (2018). MRI Classifiers Characterize Mild Traumatic Brain Injury In Symptomatic And Presymptomatic Stages And

[20] Mukhopadhyay, S., Ghosh, N., Burman, R., Panigrahi, P. K., Pratiher, S., Venkatesh, M., … Changdar, S. (2015). An optimized hyper kurtosis based modified duo-histogram equalization (HKMDHE) method for contrast enhancement purpose of low contrast human brain CT scan images. 2015 International Conference on Advances in Computing, Communications and Informatics (ICACCI). doi:10.1109/icacci.2015.7275880

[21] Niemantsverdriet, E., Struyfs, H., Van Hecke, W., Smeets, D., & Engelborghs, S. (2016). Volumetric Brain Mri Of Different Regions, Including The Hippocampus, In The Alzheimer's Disease Spectrum: A Systematic Review. Alzheimer's & Dementia, 12(7), P547–P548. doi:10.1016/j.jalz.2016.06.1071

[22] Prins, N., Benedictus, M., Binnewijzend, M., Scheltens, P., Barkhof, F., & Van der Flier, W. (2012). Cerebral blood flow, measured with ASL perfusion MRI at 3T, and structural brain changes in Alzheimer's disease. Alzheimer's & Dementia, 8(4), P737. doi:10.1016/j.jalz.2012.05.1988

[23] Sathish Kumar, L., Hariharasitaraman, S., Narayanasamy, K., Thinakaran, K., Mahalakshmi, J., & Pandimurugan, V. (2021). AlexNet approach for early stage Alzheimer's disease detection from MRI brain images. Materials Today: Proceedings. doi:10.1016/j.matpr.2021.04.415

[24] Sarraf, S., & Tofighi, G. (2016). Deep learning-based pipeline to recognize Alzheimer's disease using fMRI data. 2016 Future Technologies Conference (FTC). doi:10.1109/ftc.2016.7821697

[25] Seo, K., Pan, R., Chen, K., & Thiyyagura, P. (2017). Tracking alzheimer's disease progression by non-linear dimension reduction of brain mri features. Alzheimer's & Dementia, 13(7), P349–P350. doi:10.1016/j.jalz.2017.06.277

[26] Shi, L., Wong, L., Liu, J., Wang, D., Li, K., & Liang, P. (2019). MRI-Based Brain Volumetry In Single- And Multi-Domain Amnestic Mild Cognitive Impairment And Alzheimer's Disease. Alzheimer's & Dementia, 15(7), P712–P713. doi:10.1016/j.jalz.2019.06.2733

[27] Starr, J. M., Farrall, A. J., Armitage, P., McGurn, B., & Wardlaw, J. (2009). Blood–brain barrier permeability in Alzheimer's disease: a case–control MRI study. Psychiatry Research: Neuroimaging, 171(3), 232–241. doi:10.1016/j.pscychresns.2008.04.003

[28] Tanchi, C., Theera-Umpon, N., & Auephanwiriyakul, S. (2012). Fully automatic brain segmentation for Alzheimer's disease detection from magnetic resonance images. The 6th International Conference on Soft Computing and Intelligent Systems, and The 13th International Symposium on Advanced Intelligence Systems. doi:10.1109/scis-isis.2012.6505333

[29] Venkataramanan, S., & Kalpakam, N. V. (n.d.). Aiding the detection of Alzheimer's disease in clinical electroencephalogram recording by selective de-noising of ocular artifacts. 2004 International Conference on Communications, Circuits and Systems (IEEE Cat. No.04EX914). doi:10.1109/icccas.2004.1346340

[30] Wurts, A., Oakley, D. H., Hyman, B. T., & Samsi, S. (2020). Segmentation of Tau Stained Alzheimers Brain Tissue Using Convolutional Neural Networks. 2020 42nd Annual International Conference of the IEEE Engineering in Medicine & Biology Society (EMBC). doi:10.1109/embc44109.2020.917583

[31] Wang, S., Wang, H., Shen, Y., & Wang, X. (2018). Automatic Recognition of Mild Cognitive Impairment and Alzheimers Disease Using Ensemble based 3D Densely Connected Convolutional Networks. 2018 17th IEEE International Conference on Machine Learning and Applications (ICMLA). doi:10.1109/icmla.2018.00083

[32] Yablonskiy, D. A., Zhao, Y., Cairns, N. J., Hassenstab, J., Benzinger, T. L., Astafiev, S. V., … Morris, J. C. (2017). Gradient Echo Plural Contrast Mri Provides New Surrogate Markers Of Brain Pathology In Alzheimer's Disease. Alzheimer's & Dementia, 13(7), P127–P128. doi:10.1016/j.jalz.2017.06.2544

[33] Yablonskiy, D. A., Zhao, Y., Cairns, N. J., Hassenstab, J., Benzinger, T. L. S., Astafiev, S. V., … Morris, J. C. (2017). Gradient Echo Plural Contrast Mri Provides New Surrogate Markers Of Brain Pathology In Alzheimer's Disease. Alzheimer's & Dementia, 13(7), P780. doi:10.1016/j.jalz.2017.06.1048